Circulation, stratification and salt dispersion in a former estuary after reintroducing seawater inflow

Kranenburg, Wouter M.; Tiessen, Meinard; Blaas, Meinte; Van Veen, Nathalie

DOI
10.1016/j.ecss.2023.108221

Publication date
2023

Document Version
Final published version

Published in
Estuarine, Coastal and Shelf Science

Estuarine, Coastal and Shelf Science 282 (2023) 108221

Contents lists available at ScienceDirect

Estuarine, Coastal and Shelf Science

journal homepage: www.elsevier.com/locate/ecss

Circulation, stratification and salt dispersion in a former estuary after reintroducing seawater inflow

Wouter M. Kranenburg [a,b,*], Meinard C.H. Tiessen [a], Meinte Blaas [c], Nathalie P. Van Veen [c]

[a] Deltares, Delft, the Netherlands
[b] Hydraulic Engineering, Delft University of Technology, Delft, the Netherlands
[c] Rijkswaterstaat, Unit Water Verkeer & Leefomgeving, Lelystad, the Netherlands

ARTICLE INFO

Keywords:
Salt intrusion
Estuaries
Lakes
Circulations
Stratification
Transport

ABSTRACT

Around the world, estuaries have been partially or completely closed-off from the sea and their number may increase with rising sea levels. Concurrently, there is a trend to reintroduce seawater inflow into enclosed former estuaries for ecosystem improvement. This is also the case in the Haringvliet, a former estuary in the Rhine-Meuse Delta, closed-off in 1970 with floodgates blocking seawater inflow and regulating outflow. As the reintroduced salt water inflow can threaten fresh water intake, inflow, flushing and dispersion need to be well understood and carefully managed.

Here we investigate stratification, flow circulation and salt transport in the Haringvliet by analyzing ADCP data collected in two former tidal channels, together with salinity time series and profiles. The profiles show that the incoming water reaches the deeper parts and that the system tends to be strongly stratified. Over time, the interface levels deepen in steps, mainly coinciding with floodgate discharge events, which are strongly correlated with the primary current velocities in the channels. However, even floodgate discharges for above average Rhine discharge conditions were insufficient to quickly flush or mix the salt out of the channels. This is consistent with calculated gradient Richardson numbers, which barely get in the range of critical values.

For closed floodgates with no outward discharge, we found considerable depth-averaged upwind currents in the channels for axial winds. This reveals a dominant horizontal circulation, with downwind currents over the shallow parts and upwind currents over the deep parts of the system, explained by a local imbalance between the wind stress and pressure gradient force at both shoals and channels. This horizontal circulation is an important driver for inland salt transport, as increased salinity values were found at landward locations for seaward wind. This implies this is a condition with increased risks for fresh water availability. Analytical calculations confirmed the upwind currents in the channels can become sufficiently strong to transport salt mixed up at one side of the system to the other within the duration of a wind event. However, the current-related shear is likely not strong enough to induce interfacial mixing directly above the deep parts, and we hypothesize mixing mostly occurs when salt water reaches less deep areas after tilting of the pycnocline.

The insights from this study are relevant for other formerly enclosed estuaries for which reintroduction of seawater inflow is considered, as well as presently open systems for which (partial) closure is discussed.

1. Introduction

Around the world, numerous estuaries and tidal lagoons have been partially or completely closed-off from the sea by dams, storm surge barriers, sluices and floodgates. In South Korea, for instance, this concerns about half of the country's estuaries (Lee et al., 2011; Figueroa et al., 2021), and hundreds of estuarine dams have been built in China (Zhu et al., 2017). Examples in The Netherlands are the Lake IJssel, which is the former Southern Sea, and the Grevelingen and Haringvliet (Tönis et al., 2002), both former estuaries in the Rhine-Meuse delta closed-off as part of the Deltaworks after a major flooding in 1953 (Watson and Finkl, 1990). Besides flood risk reduction through shortening of the coastline, estuarine closures have been directed at claiming land, creating freshwater reservoirs or generating electricity (Morris, 2013). Although the attention for adverse environmental impacts of hydraulic structures is increasing and the focus in coastal engineering is

* Corresponding author. Deltares, Delft, the Netherlands.
E-mail address: wouter.kranenburg@deltares.nl (W.M. Kranenburg).

https://doi.org/10.1016/j.ecss.2023.108221
Received 6 July 2022; Received in revised form 30 December 2022; Accepted 12 January 2023
Available online 18 January 2023

shifting towards more nature based solutions, barriers and floodgates remain cost-effective measures for flood risk management (Deltacommissie, 2008) and hard structures are likely to become increasingly important to reduce coastal flood risk in densely populated areas (National Research Council, 2014). In this way, climate change and rising sea levels may lead to even more estuary closures in the future. However, for estuaries formerly closed-off with dams and floodgates, there is also a trend to partially re-open them again for limited seawater inflow, to reduce the adverse impacts of the earlier closures on water quality and ecology. In the Netherlands, the latter is apparent in plans and measures for the Lake IJssel (Project Afsluitdijk; fishmigrationriver Afsluitdijk), the Grevelingen (Project Tide Grevelingen) and the Haringvliet (Project Haringvlietsluizen). An example from South Korea is the Nakdong estuary (Jun et al., 2019). As many of these systems nowadays also function as a freshwater resource, relevant questions from a management perspective are: how far will inflowing salt spread through a system? And what measures and operational strategies are available to control the extent of the salt intrusion to safeguard freshwater availability? Against this background this study investigates the circulation, stratification and salt transport in the Haringvliet system after reintroduction of seawater inflow through the floodgates to enhance fish migration into the Rhine river.

Generally, in estuaries, with open connection to the sea, salinity intrusion and dispersion through the system are the result of a continuously changing competition between (net) inward transporting mechanisms like the estuarine circulation and tidal dispersion, and the outward transport due to the river related net outward flow (Fischer, 1972; Fischer et al., 1979). The most important contribution to the estuarine circulation is the gravitational circulation (Hansen and Rattray, 1965; Chatwin, 1976; Geyer and MacCready, 2014), the density-driven exchange flow directed inward near the bed and outward near the surface due to the sea-river salinity difference. This mechanism also generates stratification, competing with mixing primarily generated by the tidal motion. The result is a wide range of estuaries with varying levels of stratification. This is reflected in stratification-based classifications of estuaries (e.g. Valle-Levinson, 2010). An increase in freshwater discharge leads to increased outward fluxes, pushing salt outward. Simultaneously, it shortens the fresh-salt transition, thus contributing to increased baroclinic pressure gradients, gravitational circulation and stratification. A decrease in tidal energy may also lead to increased stratification and gravitational circulation, inducing increased salt intrusion if the circulation is the dominant inward transport mechanism (Geyer et al., 2000; Bowen and Geyer, 2003).

In lakes, circulation, mixing and transport are often dominated by atmospheric forcing. Wind over basins with homogeneous density and a uniform depth will initiate a water level tilting until a barotropic pressure force has developed that balances the wind force (Imberger and Hamblin, 1982). In this case, a vertical circulation will develop with downwind flow at the surface and upwind flow near the bed (Officer, 1976). For lakes with a two-layer stratification also the pycnocline will tilt, but with an opposite direction and a much larger steepness than the surface slope (Mortimer, 1953), while two vertical circulation cells will develop, the one in the lowest layer being weak as the shear stress at the interface is small. Whether a tilted pycnocline can surface at the upwind end of a lake (upwelling) is indicated by the Wedderburn number (Thompson and Imberger, 1980), which links the characteristics of the system to the ratio of the pressure force from the tilted interface and the wind force.[1] Release and time-variation of the forcing results in internal seiches (Mortimer, 1953). For basins with a homogeneous density but a shallow and a deep side, wind can drive a horizontal circulation, with (depth-averaged) downwind currents on the shallow side and upwind currents on the deep side of the basin for axial winds (Csanady, 1975; Fischer, 1976; Wong, 1994). Wind may also cause deepening of a mixed layer by turbulent entrainment mixing (Kato and Phillips, 1969; Price, 1979; Wüest and Lorke, 2003).

The circulation, stratification and mixing in estuaries can also be affected by wind. Down-estuary wind can enhance the estuarine circulation and salt intrusion and strengthen the stratification (Hansen and Rattray, 1965; Weisberg, 1976), as the down-estuary wind can enhance the subtidal vertical shear, leading to straining of the density profile (Scully et al., 2005). Up-estuary wind has the opposite effect: it inhibits and can even reverse the direction of the estuarine circulation (Purkiani et al., 2016; Coogan and Dzwonkowski, 2018; Lange et al., 2020). However, for strong down-estuary winds or moderate down-estuary winds acting on shallow water, stratification can also be reduced (Goodrich et al., 1987; Geyer, 1997). Chen and Sanford (2009) addressed this increase-then-decrease transition in the effect of down-estuary wind on stratification in their numerical study on the competition between wind straining and direct wind mixing, summarizing their results in a regime diagram spanned by the Wedderburn number and the entrainment depth to water depth ratio. Lateral and longitudinal effects of wind may also interact. Including rotational effects, Li and Li (2011) found that lateral straining of the density field by wind-driven lateral circulation offsets the longitudinal straining effect and reduces the asymmetry between the down- and up-estuary winds. Wind-driven lateral exchange can be important for transport as well: studying oxygen levels in Chesapeake bay, Scully (2010) found this to be more important for oxygen renewal than direct turbulent mixing through the pycnocline. Wind may also influence the exchange with coastal oceans through its influence on the estuary plume (Xia et al., 2011; Kang et al., 2017).

The system studied here, the Haringvliet, is a former estuary, with a bathymetry still reflecting the estuarine features of ebb and flood channels and shoals, closed-off for seawater inflow in 1970 (Ferguson, 1971), but recently reopened again for limited seawater inflow. Presently, the system also functions as fresh water resource. As the salt can threaten the freshwater availability, the inflow, flushing and dispersion of the salt water need to be well understood and carefully managed. In this paper, we study field data gathered around the experimental opening of the floodgates for seawater inflow in winter 2019–2020, aiming to answer the question when and how salt water that has entered the Haringvliet after opening the floodgates for seawater inflow is flushed out, mixed up and/or spreads through the system. Because of the related management risk, we focus particularly on the latter.

The set-up of this paper is as follows: In section 2, we describe the field site, instrumentation and data processing. Section 3 describes the results for stratification, interface displacement, depth-averaged and depth-dependent current velocities and salinity at various locations in the system and explores their relationship with the floodgate flushing discharge and the wind. To verify our interpretation of the observations, we further analyze and discuss the dynamics of the system in section 4. This is followed by a brief discussion on the implications for management of the system and points of attention for upcoming experiments. The conclusions are summarized in section 5.

2. Methods

2.1. Field site

The Haringvliet is a former estuary in the Rhine-Meuse delta (Fig. 1), closed-off with floodgates in 1970 as part of the Deltaworks to protect the South-West of the Netherlands against flooding. It presently functions as one of the two main conduits in the West of the Netherlands for the discharge of the Rhine and the Meuse towards the North Sea, the other being the Rotterdam Waterway, which has an open connection with the sea. The Haringvliet floodgates are used to regulate the seaward outflow, while keeping the seawater out. So basically, there is no flood inflow, and only a regulated outflow during ebb. For low river

[1] Note that – interestingly – in literature on wind in estuaries, the Wedderburn number is generally inversely defined as wind force over buoyancy force.

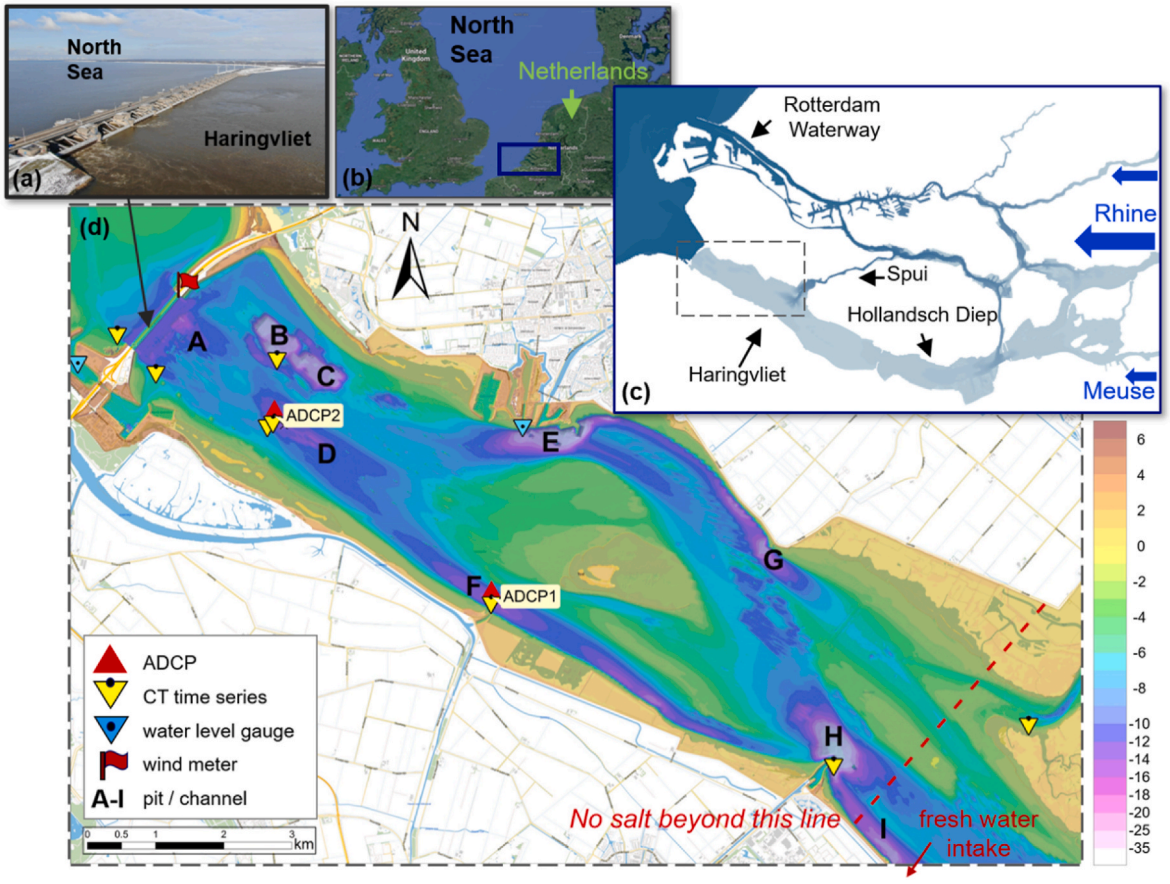

Fig. 1. The Haringvliet and the Rhine-Meuse Delta. a) Haringvliet floodgates, picture Rijkswaterstaat; b) position of Rhine-Meuse Delta in North-West Europe; c) The network of rivers and channels in the Rhine-Meuse Delta, with the Haringvliet and Rotterdam Waterway, the two main conduits of Rhine and Meuse water to the North Sea (blue shades for visualisation purposes only); d) The western part of the Haringvliet system, with bathymetry and location of instruments in the fall and winter 2019–2020. Bathymetry scale in meters with respect to reference level (NAP, the 'Normaal Amsterdams Peil', with NAP 0 m a level close to the average sea level at the North Sea). (For interpretation of the references to color in this figure legend, the reader is referred to the Web version of this article.)

discharges, the gates are fully closed also during ebb, and the water is directed to the Rotterdam Waterway to avoid salt intrusion there. After years of discussion, it was decided on the highest Dutch political levels to reintroduce a limited seawater inflow into the Haringvliet, to improve fish migration towards upriver spawning grounds. This managed seawater inflow is realized by slightly opening some of the gates during flood tides. The responsible Dutch governemental agency, Rijkswaterstaat, started experimenting with very small openings in 2018, with the idea to gradually increase the seawater inflow during the experiments to gain an understanding of the dynamics and experience in controlling the extent of the salt water intrusion. This control is important, as it was agreed upon that the sea water reintroduction will be managed in such a way that no salt will arrive in the eastern part of the system (indicated by red line in Fig. 1). This should guarantee that the opening of the gates will not affect the functioning of a major fresh water intake, which was displaced eastward specifically for the purpose of this project (location indicated in Fig. 1).

On average, the Haringvliet is about 7 m deep, but the depth variation is strong. The bathymetry, plotted in Fig. 1d for the western part of the Haringvliet, shows a big shoal and several deep channels and pits. These deep areas are the result of past tidal influence, scour near jetties and other constructions and, for areas B and C, sand mining. The deepest depression is about 45 m deep (pit H). The barrier separates the Haringvliet from the sea at the north-west side of the system by means of 17 double-door floodgates which can be lifted from the sill depth at 5.50 m below reference level (the 'Normaal Amsterdams Peil', NAP, with NAP 0 m a level close to the average sea level at the North Sea). The fresh water from the Rhine and the Meuse enters the Haringvliet via the Hollandsch Diep at the south-eastern side of the system (Fig. 1c). Besides the Hollandsch Diep, the Haringvliet is also connected to the rest of the Rhine-Meuse delta via the Spui at its northern side. Through these two connections, there is a tidal influence on the Haringvliet causing a water level fluctuation with a range up to 0.50 m, maximum (tidal range at entrance of Rotterdam Waterway is 1.0 m for the smallest neap tides up to 2.3 m for the greatest spring tides, and up to 3.0 m at the seaward side of the floodgates). Via these connections, the Haringvliet water levels can also be influenced by wind set-up at sea. During strong set-up events, the combined tide and wind set-up induced flow towards the Haringvliet via Rotterdam Waterway and Spui occasionally leads to salt water reaching the Haringvliet from the north side (called 'backward salinization') (Huismans, 2016). Here, we focus on the fate of salt coming in via the Haringvliet floodgates.

2.2. Experiment set-up and instrumentation

Up to now, the experiments on seawater inflow take place in the fall and winter season, with generally moderate to high river discharges. This is done to avoid the situation that no fresh water is available anymore for flushing in case salt inadvertently spreads too far east. In this paper, we focus on data from the 2019–2020 season. On October 9, 2019, seawater was allowed to enter the Haringvliet. This was followed by periods of active flushing and periods with closed gates.

During this period, salinity and temperature were monitored with arrays of conductivity-temperature sensors beneath floating platforms at

multiple locations in the western part of the Haringvliet. This included measurements in channel D (Fig. 1d) at 2, 8 and 13 m and at 10, 11 and 12 m (from a second array close by), in channel F at 2, 7 and 15 m and in pit H at 2, 8 and 15 m beneath the (moving) water level, all with a sampling interval of 10 min. At these locations, also vertical profiles of salinity and temperature were measured about once every two to three weeks. From August 20, 2019, until March 10, 2020, two Nortek ADCP's were deployed on bottom frames, one in channel D and one in channel F, measuring upward with bins of 50 cm and intervals of 10 and 12 min (Fig. 1d). Halfway through the deployment, at December 12, 2019, the ADCP's were recovered, cleaned, reprogrammed and redeployed. For the measurements in channel F, unfortunately only the redeployment provided useful data.

Continuous time series measurement of permanent stations included in this study are measurements of water level elevations at stations Hellevoetsluis and Stellendam-buiten, the latter on the offshore side of the floodgates (Fig. 1d), and measurements of wind speed and direction at station Haringvlietsluizen Sch1, all providing data with 10-min intervals. Also the gate operation was recorded by registering the opening height of each of the 17 gates with a 10-min interval. An overview of the data used in this study is given in Table 1.

2.3. Data processing

As a first processing step, all time series were projected on an identical time axis with 10-min intervals, spanning the period August 20, 2019, 00:00 until March 11, 2020, 00:00. For the ADCP data, this does include time interpolation, as these recordings did not start at rounded 10 min and were partly done with 12-min intervals.

Subsequently, floodgate discharges were calculated from the water level measurements seaward and landward of the floodgates and the recordings of the floodgate openings, using the weir relation:

$$Q = mA\sqrt{2g\Delta h} \tag{0.1}$$

where Q is the discharge through the floodgates, A the total floodgates opening, g the gravitational acceleration, Δh the water level difference between upstream and downstream side of the floodgates and m a tuned coefficient accounting for flow contraction, energy losses from deceleration and friction and inaccuracies from differences between the upstream and downstream water levels and the actual upstream and downstream energy head. Here, $m = 0.78$ is used, both for outflow and inflow, following the practice in our organisations for calculating the outflow discharge. This value is based on laboratory scale experiments and calibration for outward currents in the design and construction phase of the floodgates. (However, we have not been able to identify the original reference). The resulting discharge times series contained multiple smaller and larger gaps. Small gaps of only one or two data points were filled through linear interpolation. A few larger interruptions, related to gaps in the time series of the water levels at the seaside of the construction, have been filled up with floodgate discharge estimates based on operational water level predictions for those dates (Matroos) or hindcasts using those operational models.

Table 1
Overview of data used in the analysis.

#	Data-series	Source	Interval	Location
1	Water levels	LMW([a])	10 min	Station Hellevoetsluis & Station Stellendam-buiten
2	Floodgate openings		10 min	Haringvlietsluizen (gate 1–17)
3	Wind speed & direction	LMW	10 min	Station Haringvlietsluizen Sch1
4	Horizontal velocities	ADCP-measurements	10–12 min, 50 cm	ADCP1 in channel F; ADCP2 in channel D
5	Acoustic backscatter	ADCP-measurements	10–12 min, 50 cm	ADCP1 in channel F; ADCP2 in channel D
6	Salinity time series	CT-arrays below moored platforms	10 min	Platform in pit H ('Middhnsmb') Platform in channel F ('Kier1') Platforms in channel D ('Harvwt' & 'Kier3')
7	Salinity profiles	Shipboard measurements	2–3 weeks	Location in channel F ('2.3') Location in channel D ('1.6') Both right next to platforms

[*] LMW is 'Landelijk Meetnet Water', see also https://waterinfo.rws.nl.

For the velocity data from the ADCP's, the data in the most upper part of the water column, generally 1.0–1.5 m, were removed to get rid of the influence of reflection by the water surface. The primary current directions over the full record were determined by finding the direction with maximum variance, and the eastward and northward velocities were projected on axes in the primary (m-) and counterclockwise perpendicular secondary (n-) horizontal directions. After the axis rotation, the ADCP data were slightly smoothened with a boxcar filter, using 7 points in time and 3 in space. Sometimes in such analyses, the profiles are extended towards the bed and the water surface using e.g. a logarithmic and a parabolic profile, with a certain bed roughness height z_0 and a no-shear boundary condition at the surface. This is not done here, as we expect the profiles to be influenced by wind. Note that, because of this, so called 'depth-averaged velocities' are actually velocities averaged over the available part of the profile. Like the velocity profiles, also the ADCP backscatter profiles were cut off and filtered. These were used to identify strong density interfaces and to estimate the time development of the interface level. This was done by determining the local maxima in the profile of the backscatter. This can provide information on density transitions as the acoustic signal of the ADCP reflects on density interfaces due to the changes in acoustic properties. The backscatter may also be enhanced by local maxima in suspended sediment concentrations, which can occur around density interfaces due to effects of density gradients on vertical mixing. Though the 50 cm bin-size and the large scatter over time do not allow for a very accurate determination, the estimates provide insight into the interface development in the time between subsequent shipboard salinity profile measurements.

For the salinity time series, measured at fixed distances below the water level, the vertical positions of the sensors with respect to reference level were determined using the water level measurements at Hellevoetsluis. The same was done for the vertical positions of the profile measurements. Like the velocity data, salinity and wind time series have been slightly smoothened for further presentation and analysis (with filter lengths of 7 points in time, unless stated otherwise with the figures).

3. Results

3.1. Forcing conditions

3.1.1. Floodgate discharges

The calculated floodgate discharges (Fig. 2b) show a major inflow event in October 2019, followed by periods of flushing and of closed gates. Describing the discharge conditions in more detail, from the beginning of our measurement period (August 20) until October 8, the outward discharge was zero or at maximum 50 m^3/s, as the gates were closed to keep fresh water in and only slightly opened occasionally to allow a minimal flushing. On October 9, 2019, the gates were opened during flood and about 25×10^6 m^3 of salty seawater was allowed to enter the system. This inflow event was followed by periods of moderate flushing (e.g. 10/10-10/21 and 11/29-12/02), with periods of closed gates in between (e.g. 10/21-11/1 with one interpution, and 11/5–11/

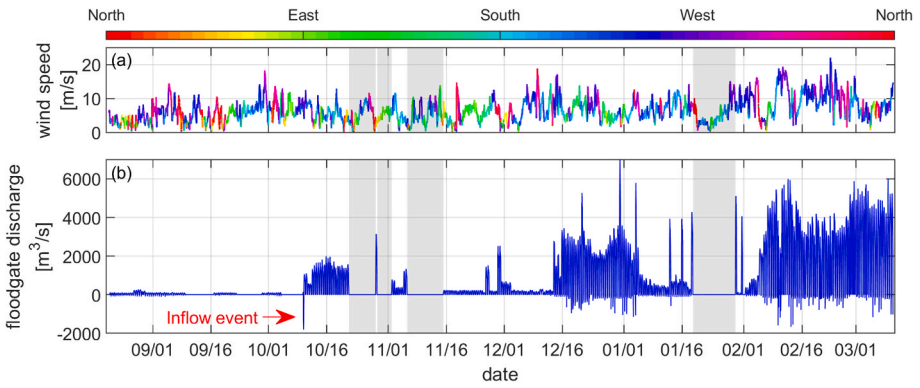

Fig. 2. Forcing conditions. Top) wind speed and direction (average of the preceeding hour, directions following meteorological convention); Bottom) Estimated discharge through the floodgates (positive is seaward). The gray shades indicate multi-day periods of closed gates after the seawater inflow event on October 9, 2019. (For interpretation of the references to color in this figure legend, the reader is referred to the Web version of this article.)

14; after November 14, some limited flushing was needed as the salt was intruding too far East). December 12 forms the start of a new period, in which significantly higher floodgate discharges occur, related to a strong increase in the Rhine discharge. In this period, a limited additional seawater inflow into the system did occur. This happened because the gates were sometimes opened some time before the moment of zero water level gradient over the gates during falling tide, or closed some time after this moment during rising tide. Between 01/13-01/18 and 01/29-02/02, experiments were carried with peak flushing rates, while the gates were closed from 01/19-01/29. An chronological overview of the floodgate discharge conditions is given in Table 2.

3.1.2. Wind

The wind speed during the measurement period (Fig. 2a) was on average 6.7 m/s, with a standard deviation of 3.4 m/s for the hourly average wind. The dominant wind direction was from the South-West. Stronger winds tend to come from westerly directions, and events with wind speeds exceeding 15 m/s have occurred at e.g. 10/01, 12/12, 02/12 and 02/26. More general information on the wind statistics for the Haringvliet based on a two year record can be found in figure A1 in the appendix.

3.2. Stratification

3.2.1. Salinity profiles and timeseries

At the start of the experiment, there was no salt present in the system except for the background salinity of the rivers Rhine and Meuse. The salinity profile measurements (Fig. 3 a,b) show that the salty seawater that came in during the inflow event on October 9 reached the deep parts of channel D as well as the more south-eastern channel F. The profiles reveal a very strong salinity stratification and sharp interfaces, with for profiles in channel D up to 20 PSU difference over just about 2 m. The interface levels are observed to deepen over time. The observations from the profiles are consistent with the time series of the deepest salinity measurements, which show a continuous presence of high salinity water from the inflow event on October 9 until January 31 for channel F (Fig. 3d) and until January 17 for channel D (Fig. 3c) at respectively 15 and 13 m below the water surface. After these moments, for a period of several days strong fluctuations are observed in the salinity time series. We explain this from the upward and downward motion of the sensors moored to the floating platforms due to the water level variation induced by the tide and wind-induced set-up at sea, which influence the Haringvliet water level through the open connection with the sea via the northern part of the Rhine Meuse Delta (Fig. 1c). The sensors move up and down through the much steadier interface with strong vertical salinity gradient, causing strong fluctuations in time. In pit H (Fig. 3e), the high salinity water is not found down to at least 15 m below the water surface. Instead, the upper 15 m are rather well-mixed, showing salinity variations of the order of but generally somewhat smaller than the near surface variations in channel F. Even though the salinity is much lower than observed in the deep pits, these observations are relevant. They indicate that salt from the reintroduced seawater inflow can end up near the surface in the eastern part of the system. This could affect fresh water availability if this water would also reach the fresh water intake. Norms for freshwater intake in The Netherlands are very strict, sometimes only allowing a chlorosity (right *y*-axis) of just 150 mg/l maximum, which equals a salinity of just 0.27 PSU.

Table 2
Overview of floodgate discharge conditions.

Period	Characterization
08/20-10/08	Floodgate discharge ≈ 0 m^3/s
10/09	Inflow event, volume $\approx 25 \times 10^6$ m^3
10/10-10/21	Moderate outward floodgate discharges
10/21-11/01	Closed gates, floodgate discharge $= 0$ m^3/s (with one interuption)
11/01–11/05	Moderate outward floodgate discharges
11/05–11/14	Closed gates, floodgate discharge $= 0$ m^3/s
11/14-11/29	Limited flushing since salt is too far east
11/29-12/02	Moderate outward floodgate discharges
12/02–12/12	Limited flushing
12/12-01/03	High outward discharges, including 3 distinct peaks; some limited seawater inflow
01/03-01/13	Moderate outward floodgate discharges
01/13-01/18	Moderat outward floodgate discharges; Experiments with 3 isolated flushing events
01/19-01/29	Closed gates, floodgate discharge $= 0$ m^3/s
01/29-02/02	Two more experiments with isolated flushing events
02/02 onward	Outward floodgate discharges quickly increased because of increasing river discharge

3.2.2. Interface displacement

The low frequency of the salinity profile measurements makes it difficult to directly relate changes in the salinity profiles to floodgate discharge and wind conditions. However, some additional insights into the behavior of the salinity profile in the time between subsequent shipboard profile measurements – though with limited quantitative accuracy – can be obtained from the backscatter-based interface level estimates (Fig. 4d). The time development of the estimated interface level shows that the deepening takes place in steps. Not too surprisingly, these steps can to a large extent be related to high floodgate discharge events (Fig. 4b), e.g. the peaks at December 21 and 31 and January 3, 12, 16 and 19. What is more surprising, is that ebb currents/flushing events with peak discharges of 5000 and even 7000 m^3/s were not sufficient to flush out all the salt from the deeper parts of the pits and channels (Fig. 4d, compare also with Fig. 3). Note that these peak discharges for

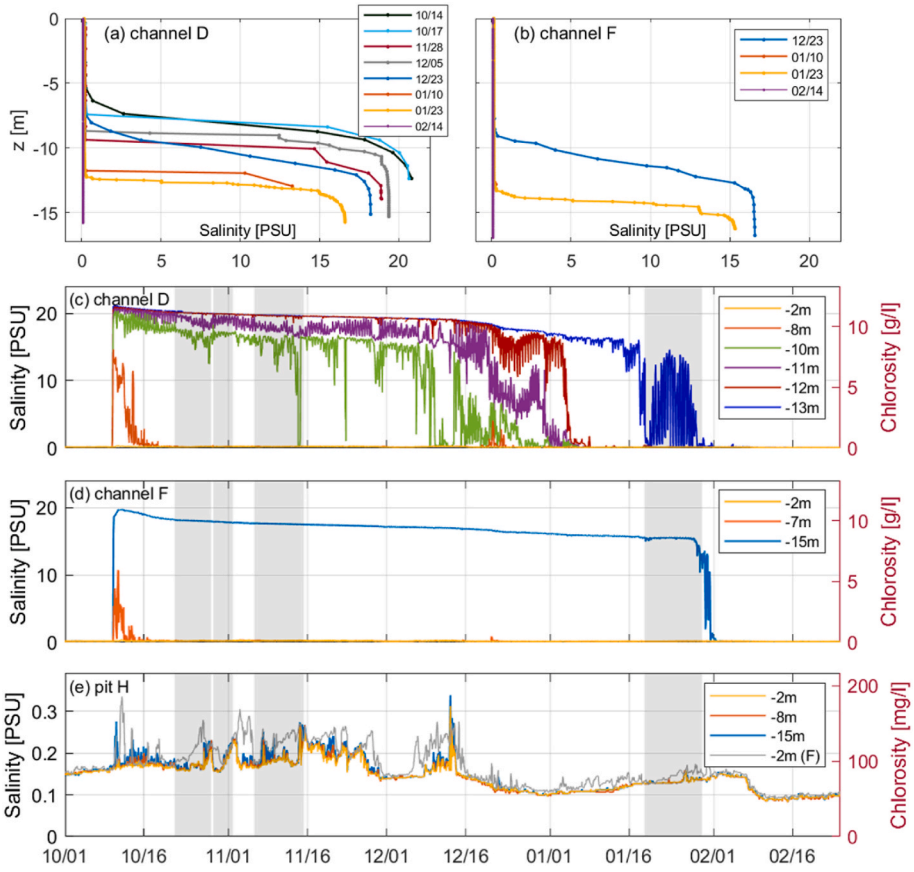

Fig. 3. Salinity. Panel a) and b) Vertical salinity profiles in channel D and channel F in the time span 2019/10/14–2020/02/14. Panel c) to e) Salinity time series at various depths in channel D, channel F and pit H, with near surface salinity in channel F also added to panel e). In a) an b) the vertical position is with respect to reference level NAP, in c) to e) with respect to the (moving) water surface. A chlorosity axis was added to the time series plots to facilitate comparison with chlorosity norms for fresh water intake and serve readers used to this measure. The relation is: S = 1.80655*Cl, with S salinity and Cl chlorosity in kg/m^3 or g/l.

the outflow during ebb are equivalent to respectively a tide average discharge of about 1600 and 2200 m^3/s. The yearly averaged discharge of Rhine and Meuse together equals about 2400 m^3/s, of which under averaged conditions about 1000 m^3/s is flowing seaward via the Haringvliet (equal to ebb peak discharges of about 3100 m^3/s). This means that salt water that has reached the deep pits and channels is difficult to remove: above averaged discharges are needed to mix or flush the salt from the deeper parts. For the lower discharges, the interface level just seemed not to be affected. This need for above average discharge conditions to remove the salt has implications for the management of the seawater inflow, which we will get back to in the discussion in section 4.2.

3.3. Current velocities

3.3.1. Currents during floodgate discharge

The depth-averaged current velocities in the primary direction (Fig. 4c) show a clear correlation with the floodgate discharges, and peaks in the floodgate discharges (Fig. 4b) are strongly reflected in peaks in the depth-averaged velocities. A correlation analysis showed that for channel F the correlation would slightly improve with a small time shift of the velocity signal of just over 10 min (see Figure A2 in the appendix). This small delay between the calculated floodgate discharges and the current velocities more upstream is consistent with the progression of a barotropic wave with a propagation speed of about 10 m/s (6000 m in 10 min), close to an estimated propagation speed $c = \sqrt{(gh)} = \sqrt{(10*12)} \approx 11$ m/s for the tidal channels in the Haringvliet. Note that the current velocities in the secondary flow direction (U_n) are very small compared to the currents in primary direction, consistent with a strong directional preference for currents in a channel.

The discharge related flow mainly takes place in the part of the profile above the interface. The current velocities below the interface are generally only very weak. A small current in opposite direction is observed to develop below the interface towards the end of the ebb flow, so while the flow above the interface is still flowing outward (Fig. 4d). This might be return flow related to relaxation of interface tilt induced by the shear of the outflow, starting as soon as the shear diminishes.

To relate these current observations to the observed interface behavior, we estimate the gradient Richardson number *Ri*, wich gives an indication of the stability of a density interface by relating the shear production and buoyancy damping of turbulence, with:

$$Ri = -\frac{g}{\rho}\frac{\partial\rho/\partial z}{(\partial u/\partial z)^2} \tag{0.2}$$

where g is the gravitational acceleration, ρ the density and u the vector velocity. We calculated *Ri* using the maximum shear in the current velocities around the estimated interface level and a salinity gradient of 10 PSU/m, estimated from Fig. 3 (a,b) and applied as representative value for the full time span stratification is present in the channels. The results (Fig. 4e) indeed indicate that only the greatest discharge and wind events will generate enough shear to start mixing salt upward, as indicated by the values in the range of the critical Richardson number (0.25–1).

Returning to the depth-averaged currents (Fig. 4c), it is also observed that the greatest floodgate discharges do not necessarily result in the greatest depth-averaged currents in the former tidal channels. The floodgate discharge at 01/03 for instance is more than 20% smaller than the discharge peak at 12/31, the velocity however is more than 10% higher and is the greatest observed velocity in the record. This is an indication the depth-averaged currents in this channel are influenced by other factors beyond just the floodgate discharge, most likely the wind, with north-westerly wind (as occurred during the 01/03 discharge peak) apparently strengthening the current towards the North-West.

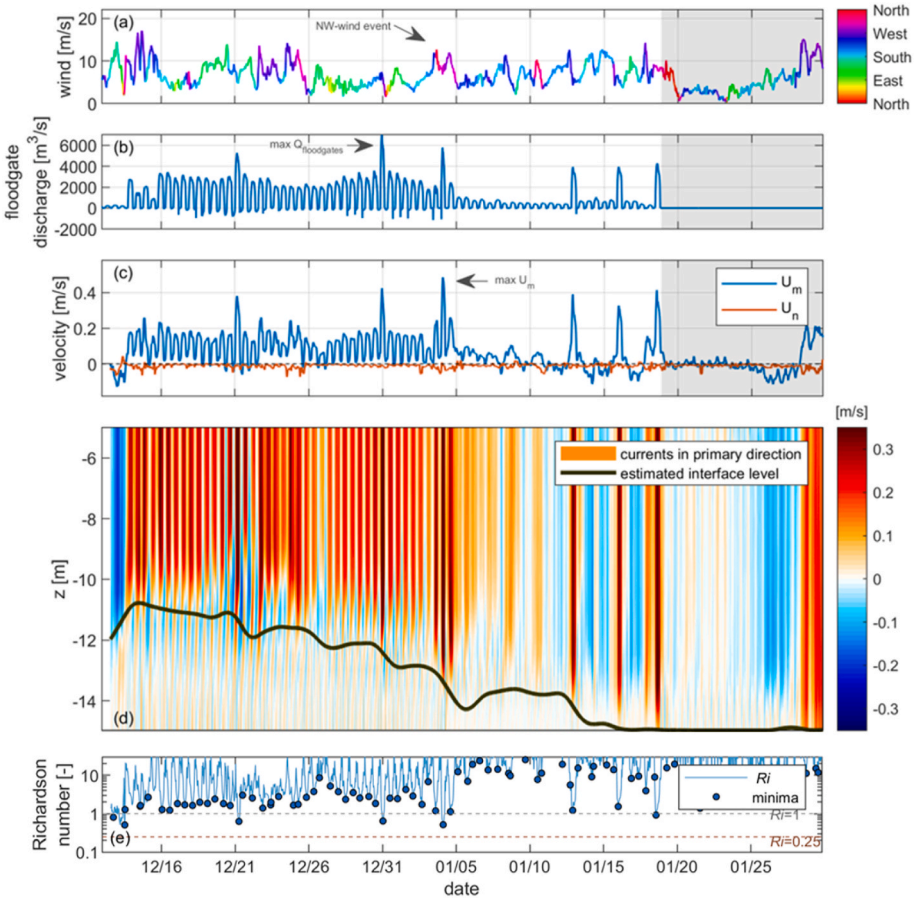

Fig. 4. Currents in channel F. Panel a) wind; b) floodgate discharge (seaward positive); c) depth-averaged currents in primary and secondary direction (U_m respectively U_n); d) current velocities in primary direction as function of depth and time, together with a backscatter based estimate of the interface level; e) estimated gradient Richardson number.

3.3.2. *Currents under influence of wind*

To better understand the wind-influence, velocity profiles are studied for situations with wind, but with no (or almost zero) discharge through the floodgates (Fig. 5). In cases of wind more or less along the main direction of the Haringvliet (NW-SE), for both ADCPs upwind directed currents are observed over a major part of the vertical profile, and the depth-averaged current velocity is clearly non-zero. Furthermore, except maybe for ADCP1 on December 13, the profiles do not show the vertical circulations which we may expect for a two-layer system forced by wind, related to the tilting of the interface and baroclinic pressure forces (see introduction). As a steady non-zero depth averaged current can only exist with a compensating flow elsewhere, these observations may indicate the generation of a horizontal circulation in the system in the case of along directional wind, which also dominates over potential vertical circulations related to the presence of the density interface.

Further studying the depth-averaged velocities at times of closed floodgates, we found both for channel D and F a negative correlation between the primary component of the depth-averaged currents (direction respectively 308 and 303° with respect to North, which is about the longitudinal direction of the Haringvliet) and the component of the wind in this same direction. This clearly indicates the presence of a net upwind current for wind in axial direction of the system. This correlation became even stronger with the current signal shifted in time or using the wind averaged over the preceding 3 or 6 h. It also improves when using the wind component in a slightly shifted direction (see correlation graphs in appendix, Figure A2). Summarizing these observations, Fig. 6a shows for channel F the relation between the primary component of the depth-averaged current and the component of the wind over the 3 preceeding hours in a direction 10° shifted with respect to the primary flow direction. Data points for north-westerly and south-easterly winds have been highlighted, further illustrating the observation of upwind currents, one of the key results of this study.

These observations on the depth-averaged currents in channel F point at a horizontal circulation in the Haringvliet system, which can be explained in line with Csanady (1975) and Fischer (1976): the wind leads to wind shear stress and a water level set-up at the downwind side of the lake. However, in the deeper parts the stress divergence will be too small to balance the pressure gradient, generating an upwind current in the former tidal channels which increases until the bottom stress has become sufficient (while meanwhile the set-up is also decreasing a bit) to establish a balance. Over the shoals, the forcing by the wind stress wins out over the forcing by the pressure gradient, driving a downwind current over the shoals. This is schematically shown in Fig. 8 (topview). The large portion of shallow area then explains the significant magnitude of the wind-induced currents in the channels. This relation is particularly strong for the deep and relatively narrow channel F, where axial winds of only 8 m/s can already generate currents of 0.1 m/s. For channel D, the relation is less strong, but the behavior is similar.

To see how this current might be affected by vertical circulations or might be different for situations with or without salt water present in the channels, we also study the current at 6.0 m depth (Fig. 6b). This level is chosen such that it is always above the interface level if salt is present in the system, but otherwise quite arbitrary. At this level the observations are very similar, and also during the time strong stratification is present in channels D and F (purple dots, data acquired between October 9 and January 30), the behavior of the current velocities at this level does not significantly differ from the behavior of the depth-averaged current.

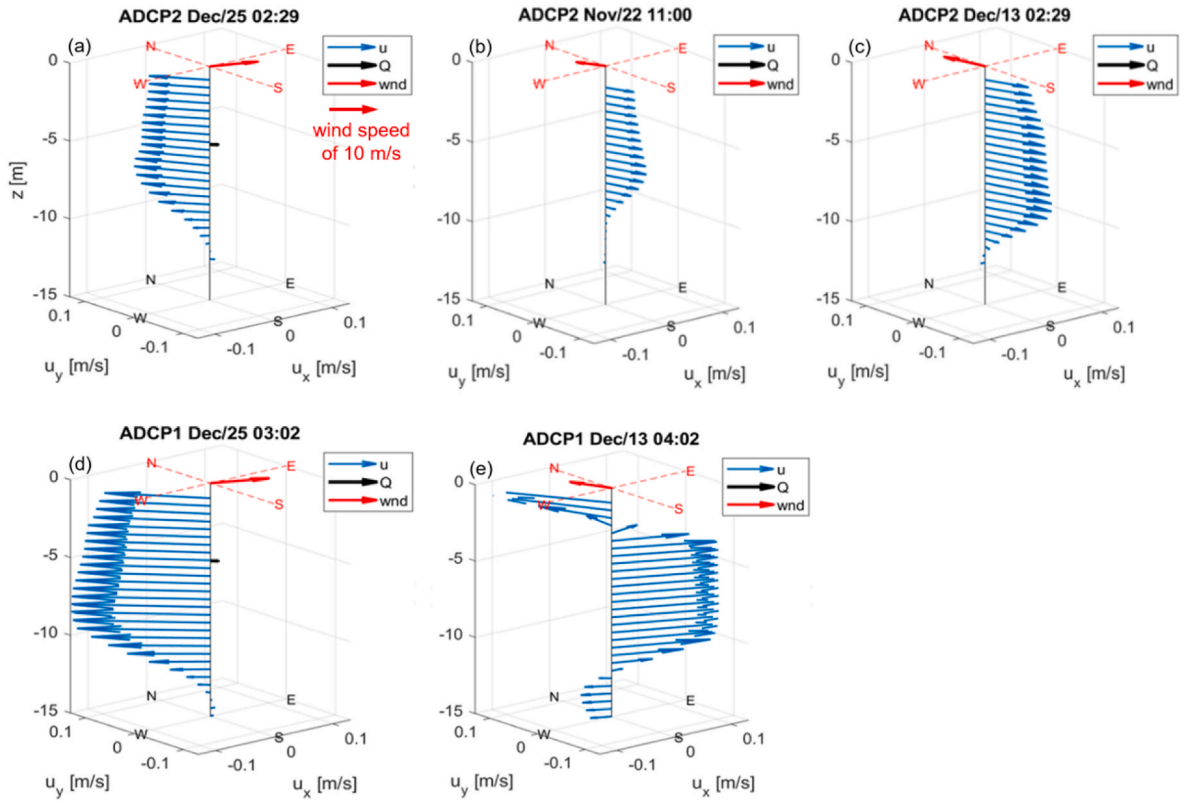

Fig. 5. Current velocity profiles. Panel a–c) profiles for ADCP2 in channel D; Panel d&e) profiles for ADCP1 in channel F; u_x and u_y are the eastward respectively northward flow velocity component. Red arrows indicate the wind forcing. For the cases shown here, the floodgate discharge (black arrow) is absent or very small (December 25). (For interpretation of the references to color in this figure legend, the reader is referred to the Web version of this article.)

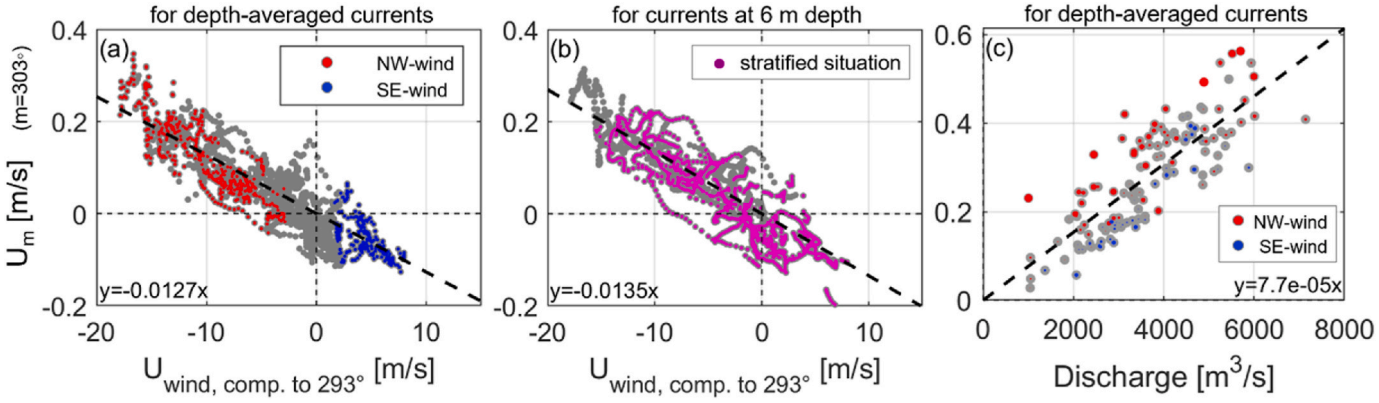

Fig. 6. Relation currents-wind and currents-discharge for channel F. Panel a) Depth-averaged current component in primary flow direction (303°) against the wind component towards 293° with respect to North, for times of closed gates; b) The same, but now for currents at 6.0 m deep; c) Depth-averaged current component in primary flow direction against the floodgate discharge. Red and blue dots indicate cases with wind from the north-west respectively south-east, their magnitude indicates the relative wind strength. All panels: 'wind' concerns the wind averaged over the 3 preceeding hours. (For interpretation of the references to color in this figure legend, the reader is referred to the Web version of this article.)

Internal seiches and vertical circulations might occur in the system, but this observation underlines that the horizontal circulation is strongly dominant.

Finally, the wind-induced upwind current contribution also affects the flow velocities when the floodgates are open. In Fig. 6c we see wind from the North-West enhancing currents towards the North-West and wind from the South-East reducing the north-westward currents, in line with the observation from Fig. 4c.

3.4. Near-surface salinity

We study the behavior of the near-surface salinity and its relation with wind forcing by looking into the rate of change of the salinity for the part of the time record with both closed gates and salt present in the deeper parts of (at least) channel F. As mentioned in the introduction, we do this to get insight in the dispersion of salt still present in the system after gate closure at times of low river discharge, so when no water is available for flushing. This is relevant, as the salt may threaten fresh water availability if it is transported too far eastward, towards the freshwater intake (see Fig. 1).

The analysis builds upon an earlier analysis of near-surface chlorosity signals by Fioole (2020). Firstly, using time series of salinity with moving averages over 740 min, we generated 10-min interval time series for the rate of change of the salinity. Using the 10-min interval time series of the wind averaged over the preceeding 3 h, we assigned each sample to a wind bin based on wind speed and direction. Subsequently, we determined the average rate of change for each bin.

The results for average change per wind bin are shown in Fig. 7a and b for near-surface salinity in channel F and pit H. From these figures, it can be observed that both in channel F and pit H, south-easterly winds tend to lead to an increasing salinity. This increase is the strongest for pit H. For this pit also easterly and north-easterly wind contribute to increasing salinity. For channel F, we generally find northerly and north-westerly winds leading to decreasing salinity, especially when the wind is moderate. These observations indicates that the wind-induced upwind current towards the South-East during south-easterly wind is an important driver for inland transport of salt mixed up elsewhere. This is the second most important result of this study. The wind-current-transport relation is further illustrated in Fig. 7c for the period of closed floodgates between November 6 and 15. For this figure we use the depth-averaged currents in channel D, as no flow velocity measurements are available for channel F for this moment, and did apply some further smoothing to obtain a more clear visualisation. Firstly, we see again that the component of the wind in primary flow direction clearly correlates with currents in the opposite direction ($u_{w,m}$ correlated with $-U_m$). Secondly, the periods this current is directed to the South-East (so when $-U_m$ is positive) coincide rather well with periods of increasing near-surface salinity in pit H, see for instance November 7 and 14. This is also the case for most of the instances of increasing salinity in channel F. However, it is interesting to observe the increasing salinity in channel F on November 9, which coincides with rather strong absolute wind speeds, but does not translate in an major increase of the salinity in pit H. Apparently, salt is being mixed up under influence of the north-westerly wind but hindered from transport towards pit H by the increasingly strong flow velocity in north-westward direction in the channels. Finally, note that an average increase of the near-surface salinity of only 3×10^{-3} PSU/hour or in terms of chlorosity 1.7 mg/l, as found for southeasterly wind of 10 m/s (Fig. 7b), might seem small. However, this means a wind event of a day may well cause an increase of over 40 mg/l. Considering the background chlorosity due to the salt content of river water can be around 100 mg/l, an event of southeasterly wind could quickly cause the near-surface salinity in pit H to exceed the drinking water norms. This is also what happened on November 14 (see Fig. 3e), which is why the responsible water management agency initiated a limited flushing directly after this event (see Fig. 2).

4. Discussion

4.1. Evaluation of the system dynamics

4.1.1. Wind-induced currents

Combining the observations, we explain the increase in near-surface salinity in the landward, more south-eastern part of the Haringvliet system for conditions with south-easterly winds, from inland directed transport by a wind-driven horizontal circulation with upwind currents over the deeper parts of the system for seaward wind. This horizontal circulation is then explained by a local imbalance between the influence of wind stress and set-up and the presence of large areas with shallow water depths.

To verify this explanation, we now analyze elements of these dynamics quantitatively. The first question is: can we indeed explain the south-eastward currents with magnitudes as observed in channel F from the local imbalance between wind stress and pressure gradient influence? To answer this, we consider the momentum balance in longitudinal direction of the system, simplified to a depth-averaged balance neglecting advective acceleration, Coriolis and baroclinic effects:

$$0 = -\rho_w g \frac{\partial \zeta}{\partial m} + \frac{\tau_{w,m} - \tau_{b,m}}{H + \zeta} \tag{0.3}$$

with ζ the water level elevation, m the coordinate in longitudinal direction, τ_w the wind stress, τ_b the bottom stress, H the averaged water depth, ρ_w the density of water, g the gravitational acceleration and the stresses at the surface and the bed given by respectively:

$$\begin{aligned} \tau_{w,m} &= \rho_a C_D |U_{10}| U_{10,m} \\ \tau_{b,m} &= \rho_w c_f |U| U_m \end{aligned} \tag{0.4}$$

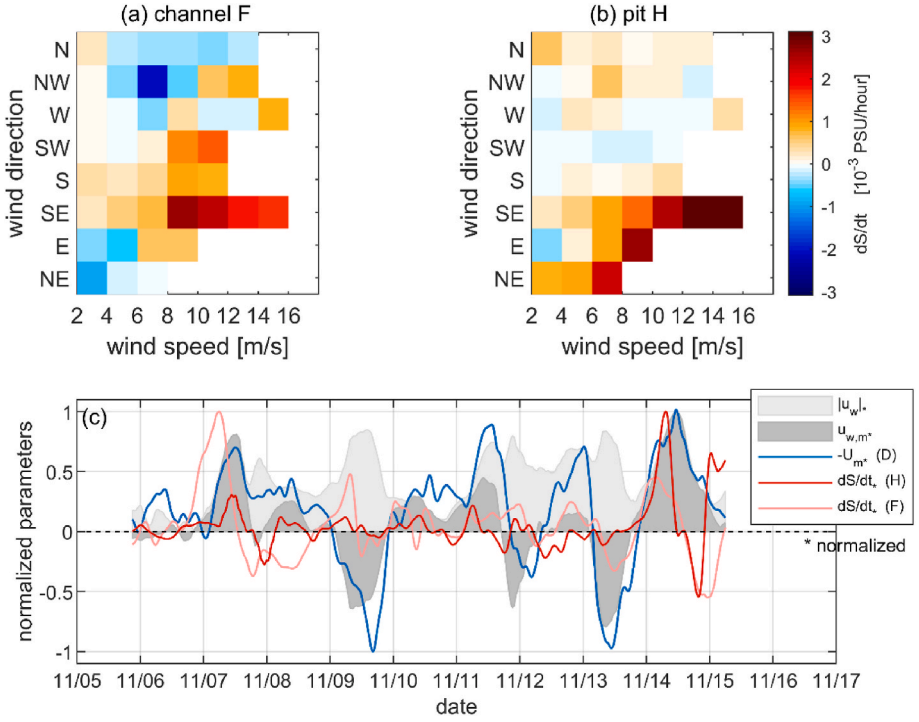

Fig. 7. (a) and (b): Averaged rate of change of near-surface salinity at 2 m below the water surface in respectively channel F (a) and pit H (b) as function of wind speed and direction the wind is coming from, over the periods with closed floodgates and salt present in the deeper parts. South-easterly winds clearly tends to lead to increasing salinity both in channel F and pit H, as indicated by the red colors. (c) Time series of the wind speed $|u_w|$ (light gray), the wind component in the primary flow direction $u_{w,m}$ (gray) (positive meaning wind towards the North-West), and the depth-averaged current component in channel D in opposite direction ($-U_m$, blue, in opposite direction to highlight the correlation between $u_{w,m}$ and $-U_m$). Red and light red lines: the rate of change $\partial S/\partial t$ of the near-surface salinity in pit H (red) and channel F (light red). All parameters except $u_{w,m}$ have been normalized by dividing them by their maximum value occurring in the plotted time span. Wind component $u_{w,m}$ has been normalized using the maximum wind speed. A salinity change of $3*10^{-3}$ PSU/hour equals a chlorosity change of 1.7 mg/l/hour. (For interpretation of the references to color in this figure legend, the reader is referred to the Web version of this article.)

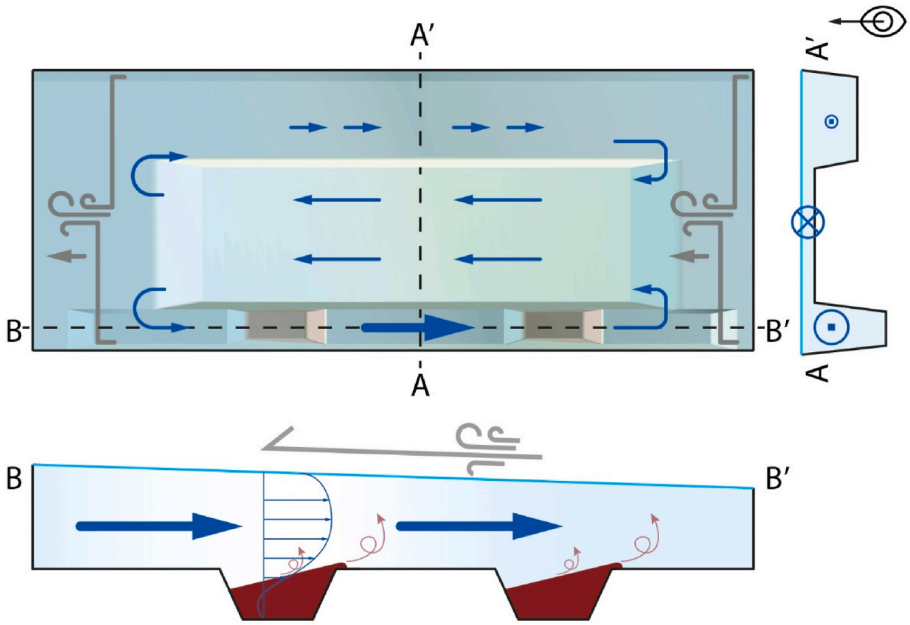

Fig. 8. Conceptual figure with topview (top left), lateral crossection AA' (top right) and longitudinal crosssection BB' (bottom). Wind in longitudinal direction drives a horizontal circulation with downwind currents over the shallow part in the middle and upwind currents over the deeper parts, in particular the deep channel on the south side. When salt is present in the system, these currents can induce upwind salt transport, as observed in this study. For this, salt needs to be mixed upward from the deepest parts of the channel. We hypothesize the mixing mostly occurs when salt water – due to tilting of the pycnocline – reaches less deep parts of the channel, where it is subsequently more easily entrained by the wind-induced circulation.

with ρ_a the air density, C_D the wind friction coefficient, U_{10} the wind velocity at 10 m height, c_f the bottom friction coefficient and U the depth-averaged flow velocity. With this, we can estimate the current in a channel and over a shallow shoal by applying the momentum balance for both. For this we assume the water level and its gradient laterally uniform, so identical in the channel and over the adjacent shoal. With one channel and one shoal, this yields three unknowns ($\frac{\partial \zeta}{\partial m}; U_{m,1}; U_{m,2}$), where $U_{m,1}$ and $U_{m,2}$ are respectively the depth-averaged velocity in the channel and above the shoal. Additional information is provided by a continuity equation stating that the joint longitudinal volume flux over the shoal(s) and through the channel(s) equals zero:

$$0 = U_{m,1}A_1 + U_{m,2}A_2 \tag{0.5}$$

where A_1 and A_2 are the cross-sectional areas above the deep and the shallow part. Using this, we estimate the flow velocities for a cross section over channel F, the shoal and the northern channel (so three parts) perpendicular to the primary flow direction in channel F. A schematic picture of the situation is given in Fig. 8. For our calculation, we schematize channel F as a rectangular channel of 0.5 km wide and 14 m deep, the shoal as 2.5 km wide and 2 m deep and the northern channel as 1.5 km wide and 10 m deep. With $\rho_a = 1.2$ kg/m^3, $\rho_w = 1000$ kg/m^3, $C_D = 1.5 \times 10^{-3}$ (Wüest and Lorke, 2003), $c_f = 3 \times 10^{-3}$ (a common value in estuarine literature) and a 10 m/s wind towards the north-west, this yields currents of −0.15 m/s in channel F, 0.22 m/s over the shoal and −0.01 m/s in the northern channel and a water level gradient of 1.8 mm/km. Although the wind-current relation of $U_m = -0.015\ U_{w,m}$ that in this way can be determined for channel F is somewhat steeper than the relation found from the data ($U_m = -0.0127\ U_{w,m}$, see Fig. 6), and assumptions and estimates made for this calculation are simplifications, the calculated and observed flow velocity are of the same order of magnitude, which supports the earlier explanation on the wind-driven horizontal circulation. Also the observed increase of the (absolute) wind-current correlation with a time shift related to averaging over multiple preceeding hours, fits in the picture, as the pressure gradient driving the upwind currents needs time to build up.

Note that the strength of the horizontal circulation would increase with increasing difference between shoal and channel depth. This is in line with Hunter and Hearn (1987), Hearn et al. (1987) and Signell et al. (1990), who studied the contribution of depth-variation-related horizontal circulation to the total wind-driven circulation for elongated water bodies with uniform density. Using an analytical model, more elaborate than our approach above, and also considering vertical profiles of the horizontal flow velocity for various eddy viscosity profiles, Hunter and Hearn (1987) found that the relative importance of the depth-integrated, horizontal circulation over the vertically varying (overturning) circulation increases with increasing variance of the depth distribution of the water body and with decreasing bottom roughness. In line with this, Signell et al. (1990) found that the wind-driven circulation decreases under influence of waves due to wave-induced increase of the bottom drag. Hunter and Hearn (1987) also found that for natural bathymetries, the horizontal circulation is generally dominant and did account for over 85% of the total circulation in the examples they investigated. So, a strong horizontal circulation in this elongated former estuary with strong depth variation is in line with literature.

Concerning vertical circulation, note the measurements were taken at locations near the deepest parts of channel/pit D, F and H, which are separated from each other by sills at around 9 m (D to F) and 4.5 m (F to H) depth. As a result, even though the measurements show a significant salinity gradient at 15 m depth between F and H, there is no large scale baroclinic exchange flow taking place in the system. Baroclinic flows will play a role when the salt water initially enters and spreads through the system. They also do when salt water may flow to another channel after reaching the sill level due to tilting of the pycnocline. Within the channels, vertical circulations from baroclinic effects may be present, but are significantly smaller than the wind-induced horizontal circulations, as observed in section 3.3.

4.1.2. Current induced transport

The next question is whether the wind-driven current would be able to transport salt mixed up from channel D and F towards area H in the time span of a wind event. With a flow velocity of 0.1 m/s for 8 m/s south-easterly wind and a distance from the CTD locations in channel F and D to area H of 5 respectively 9 km, salt mixed up from channel F and D could arrive in area H within 14 (from F) to 25 (from D) hours. As this is in the range of the duration of a wind event, the answer is positive.

4.1.3. Mixing

A more complicated question is: how and under what conditions is the salt that is transported south-eastward by the upwind current priorly transported upward from the larger depths? Does that happen through

mixing related to the wind-driven current, or rather through direct mixed layer deepening by wind-induced turbulence or other mechanisms? Clearly in this data record neither of these processes is able to fully mix the water column, as stratification persists also beyond strong axial wind events like on December 13, 2019. However, note that the observed upper layer salinity increase is only small, and even though the stratification is very strong, the direct or indirect wind-induced turbulence might be able to start entraining some salt from the lower layer.

Increasing near-surface salinity found in channel D for situations without a distinct current suggest mixing directly caused by wind-induced turbulence. Also exploratory estimates made using a 1D-vertical numerical model and the expression by Price (1979) for growth of the mixed layer depth suggest that, even for this case of strong stratification of over 15 PSU at 15 m depth, winds of only 8 m/s with a duration of a day would be able to start eating into the lower layer and mix a limited amount of salt upward. However, preliminary results from a 3D numerical model under development indicate that during closed gates, upward mixing mostly coincides with events of moderate to strong wind-induced horizontal circulation. In those cases mixing mainly seems to occur when water from the deepest parts of the channels is reaching less deep parts, in particular the shallower saddle points between two channels or pits, as a result of tilting of the pycnocline against the wind direction. Although the interface/upwelling never reaches the surface, the salt seems to be easily entrained at these shallower locations by the wind-induced current, which presumably also experiences significantly more bottom induced turbulence at these shallower locations. This explanation also makes sense in the light of the results for the Richardson number in Fig. 4e, which suggest that flow velocities of about 0.15 m/s (as may be induced by wind around 10 m/s) are not strong enough to destabilize the interface directly through shear-induced interfacial mixing right above the deepest part of the channel. We therefore hypothesize mixing mainly takes place when a thin layer of salt water is generated on slopes or saddle points after tilting of the pycnocline. This hypothesis is also indicated in the schematic of Fig. 8. Clearly, to further pinpoint the most risky conditions for salt dispersion, the exact mechanism of mixing deserves further attention, and the hypothesis might be tested with salinity data from the saddle points and an in-depth modelling study.

4.2. Implications of the findings

4.2.1. Effectiveness of flushing

The findings on flushing indicate that large discharges are needed to flush the channels and pits, and complete removal of the saline water from deeper parts of the basin in a single flush-event does not occur. A floodgate peak discharge of 7000 m^3/s results in significant water motion far into the basin with current velocities of up to 0.4 m/s in channel F. However, even for this condition there is only a limited lowering of the pycnocline of several decimeters (Fig. 4). Furthermore, 7000 m^3/s is a relatively large peak floodgate discharge and belongs to river discharges well above average. In the Haringvliet, such a large discharge is not readily available at the end of the winter season. However, originally intense flushing was the expected management strategy to get rid of the saltwater at the start of the growing season (springtime). As observed in sections 3.2, the salinity can be flushed out over a longer period of time, with help of both discharge and wind. However, this is likely to generally take weeks to months, as was the case here. The consequence would be that the operator would need to start flushing well before closing the gates for a period of low river discharge, and that during this period no or very limited additional saline water can be allowed to enter the system. This would hamper the possibility for fish migration, the actual aim of the gate opening. Therefore, it has been concluded that this flushing is not a very suitable approach and the strategy-explorations are shifting on one side to how to manage saline water that remains in the Haringvliet during the summer period, and on the other side to finding 'dynamic equilibria', i.e. floodgate operations in which from the beginning of the gate open season, inward salt transport during sluice opening equals the outward transport during the subsequent ebb flow. For the first strategy, the key process question is how salt water spreads through the system as a result of various forcing conditions. The related management question is which risks this provides for the freshwater intakes and how too much transport in their direction could be managed/mitigated.

4.2.2. Risk imposed by wind-induced flow and transport

This dataset provides evidence of horizontal wind-induced currents that can result in signficant transport of saline water. At times of closed gates, south-easterly winds can cause an increase of near-surface salinity at the locations in the south-east part of the system. As there is a fresh water intake near the most south-eastern CTD-location to supply fresh water for agriculture and industry, this is unwanted and a main risk, as periods of moderate easterly winds are not uncommon during periods of low river discharge and large fresh water demands. It is however a complicated and challenging situation to manage, as the primary means of managing such a situation would be to open the Haringvliet floodgates during ebb, discharge water from the Haringvliet into the North Sea, and push back the saline water from the south-eastern part towards the north-western part of the former estuary. However, this requires a certain fresh water discharge, which – especially during dry and summer conditions – is not always available. On the other hand, the problem concerns only salt mixed up to the upper layer, which is much more easily flushed than the deeper layer. So from a management perspective it is now relevant to determine, focused on the upper layer, how much discharge would be needed to compensate the wind-induced current, or how quickly salt that has arrived in the upper layer near the fresh water intake can be flushed out again with a given discharge after periods of south-easterly wind. This is especially relevant in light of the finding on flushing, which makes it highly unlikely that the Haringvliet will be devoid of saline water in the deeper parts of the former estuary at the start of the growing season.

4.2.3. Further needs for future management strategies

The future strategy is likely to evolve towards a more dynamic management during the entire yearly cycle of discharge rates and water demands, which might mean an adaptive approach regarding floodgate operation, dependent on local salt intrusion conditions in combination with occurring or expected changes in river discharge and wind. This requires a further enhanced understanding of the relations between forcing of the system (through wind, discharge, floodgate opening and salinity at the seaside) and its response. Next to the questions mentioned above, this also concerns the relations at the Haringvliet floodgates themselves. Although the relation between floodgate openings and outgoing discharge rates have been validated in the past, for this complex structure they are not necessarily the same for the inward discharge. Furthermore, in the presence of stratification, the relation between floodgate discharge and salinity flux is not straightforward. Therefore, the dynamics around the structure itself and determination of the amount of salt transported inward during gate opening are a point of attention towards the future.

4.2.4. Wider relevance

This paper focused on salt dispersion in a former estuary after reintroducing limited seawater inflow. This reintroduction fits in a trend of discussions to partially re-open former estuaries, closed-off in the past by dams and barriers, to reduce the adverse impacts of the earlier closures on water quality and ecology and potentially even restore ecosystems. From that perspective, this project in the Haringvliet has a wider relevance. It may also be relevant for other enclosed former estuaries, fresh water lakes or channels experiencing salt intrusion, through seepage, locks or any other cause.

Firstly, note that this very limited reopening reintroduces the inflow of salt into this system, but is not nearly enough to reintroduce the tidal

energy that can mix the water column facilitating outward transport. The result is a system with a strong stratification. In combination with the bathymetry of a former estuary with deep channels and shallow shoals, this leads to a pathway of relatively plain inland directed transport. For systems for which reintroduction of seawater inflow is being discussed, it is relevant to find out if tipping points exist after which salt intrusion will decrease with increasing seawater inflow. For the matter, such effects on salt intrusion are also relevant for systems for which partial closure is being discussed, like the Hudson (see Orton and Ralston, 2018; Ralston, 2022; Chen and Orton, under revision). Considering the effects of a storm surge barrier for New York Harbor, Ralston (2022) found increased drag and tidal velocities through the barrier opening. This locally enhances the salinity mixing, but it also reduces the tidal amplitudes upstream of the barrier, which results in decreasing salinity mixing, increasing stratification and increasing salt intrusion length inside the estuary. So considering either partial reopening or closure of a system, in both cases not only the volume exchange but also the energy exchange is effected, and these two may have opposite effects on the salt intrusion.

Secondly, the limited reopening, in this case improving fish migration, might also have less favourable ecological effects, for instance generation of anaerobic conditions in deeper parts related to stratification, or potentially high stress levels for bentic organisms related through strong variations of the salinity levels over time. Finally, note that from a management perspective the presence of salt is primarily an issue because of the fresh water storage function of the system. Although the main reason for closing-off this estuary was coastal safety, this has been an important function eversince. Functions of systems change over time, sometimes steering, sometimes following developments.

5. Conclusions

We investigated the stratification, current patterns and salt transport in a former estuary after reintroduction of a limited seawater inflow. This salt water enters the system through floodgates that usually block seawater inflow and are used to regulate the fresh water outflow. For this study, velocity measurements from ADCPs in two former tidal channels were analyzed, together with salinity time series and profiles.

We found that the inflowing salt water reaches the deeper parts of the system and causes a strong stratification. Following the inflow event, the interface levels deepen over time in steps, which mainly coincide with floodgate discharge events. The floodgate discharges are strongly correlated to the current velocities in the channels. However, even floodgate discharges for above average Rhine discharge conditions are insufficient to quickly flush or mix the salt out of the channels and pits. This is consistent with calculated gradient Richardson numbers, which barely get in the range of critical values, indicating that even for high discharges the shear production of turbulence is insufficient to quickly break down the stratification.

For closed gates, the flow velocities are mainly determined by the wind, and considerable upwind (depth-averaged) currents are found in the former tidal channels for wind in the system's longitudinal direction. These observations indicate the presence of a relatively strong horizontal circulation in the Haringvliet system, dominant over potential vertical circulations in two layer systems forced by wind. This horizontal circulation is explained by the combined presence of large shallow areas in the system and a local imbalance between the influence of wind stress and set-up both in the channels and over the shoals, leading to downwind currents over the shallow parts and considerable upwind currents through the deep and narrow channels. These upwind currents are an important mechanism for inland salt transport, as near-surface salinity values at landward locations increase during seaward wind. We verified our explanation of the observations with analytical calculations, which confirmed that the wind-driven currents in the channels can indeed become sufficiently strong to transport salt mixed up from the deep channels and pits towards the landward locations in the time span of a wind event. However, the current-related shear is not likely to be strong enough to induce interfacial mixing directly above the deepest parts of the channels. We hypothesize mixing mainly takes place when a thin layer of salt water is generated on slopes or saddle points after tilting of the pycnocline.

The management implications of the findings on flushing are that the water manager cannot relly on the possibility to quickly flush the system in times of decreasing river discharges to get rid of the salt in preparation of a period of low river discharge and closed gates. The findings on the upwind currents in the channels for axial wind and its role in salt transport imply that in case salt is still present in the deeper parts of the system at times of low river discharge and closed gates, seaward wind conditions compose a significant risk for unwanted landward transport of saline water, threathening the fresh water intakes at the inland side of the system.

Reintroduction of seawater inflow for ecosystem restoration is considered for more enclosed former estuaries. At the same time more estuaries may be partially or completely closed-off from the sea in response to sea level rise. In that perspective, this seawater reintroduction project in the former Haringvliet estuary and the results of this study are expected to be relevant for other systems as well.

CRediT authorship contribution statement

Wouter M. Kranenburg: Writing – review & editing, Writing – original draft, Visualization, Validation, Methodology, Investigation, Funding acquisition, Formal analysis, Data curation, Conceptualization. **Meinard C.H. Tiessen:** Writing – review & editing, Writing – original draft, Resources, Project administration, Data curation, Conceptualization. **Meinte Blaas:** Writing – review & editing, Methodology, Funding acquisition, Conceptualization. **Nathalie P. Van Veen:** Resources, Project administration, Methodology, Writing – review & editing.

Declaration of competing interest

The authors declare that they have no known competing financial interests or personal relationships that could have appeared to influence the work reported in this paper.

Data availability

Data will be made available on request.

Acknowledgements

The data used in this study have been acquired by Rijkswaterstaat as part of the Rijkswaterstaat project 'Implementatie Kierbesluit'. The original data analyses at the basis of this paper were part of projects commissioned to Deltares by Rijkswaterstaat, notably Deltares project 2020-11205272-021, under the KPP agreement 2020 (Kranenburg, 2020). We thankfully acknowledge the contribution of multiple people at Rijkswaterstaat and Rijkswaterstaat contractors to various elements relevant for the realization of this study, notably Aad Fioole, Jan-Willem Mol, Karin Stone, Marijn Helvert and Sacha de Goederen. We also thank the two anonymous reviewers for their comments and suggestions.

Appendix

A.1 Wind statistics

Wind statistics for the Haringvliet based on a two year record show a dominant wind direction from south-west to west-south-west (figure A1). Stronger winds tend to come from the west-south-west to north-westerly directions.

A.2 Correlations

Studying the relations between currents in primary direction, floodgate discharges and wind, we investigated how correlations between the time series would change with time shifts of the velocity signal, the use of wind speed averaged over the preceeding 1, 3 or 6 h instead of 10 min (which basically also includes a time shift), or projection of the wind on an axis for various direction. The results are shown in (figure A2).

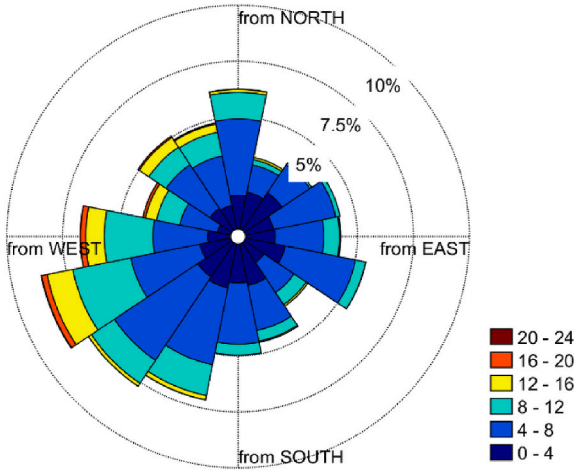

Fig. A1. Wind rose based on a two year wind record for station Haringvlietsluizen Sch1. The legend shows wind speed bins in m/s.

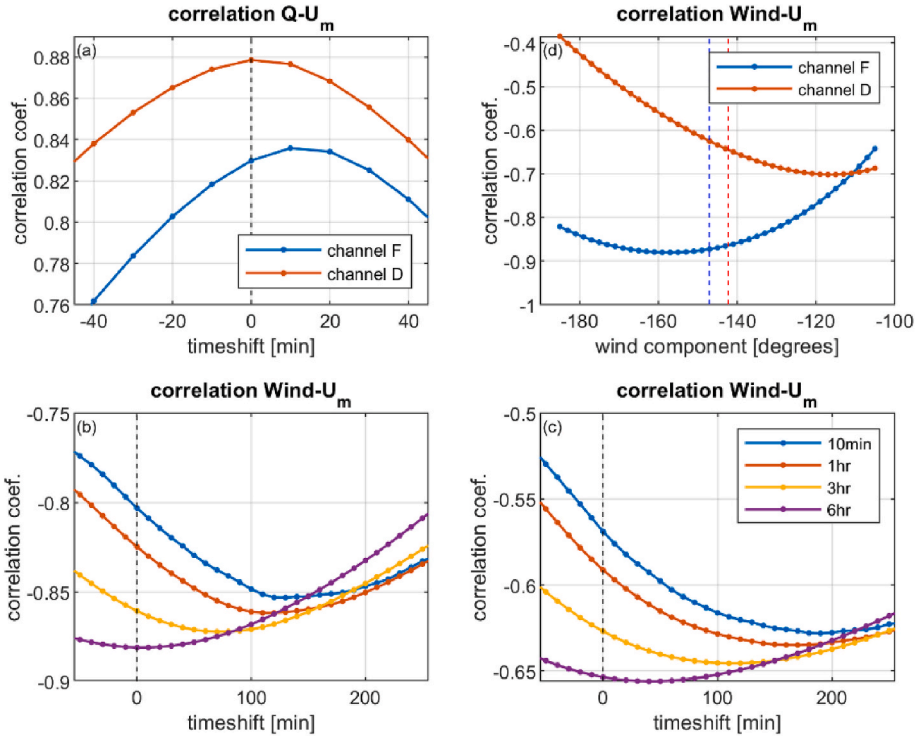

Fig. A2. Correlation coefficients for the correlation between depth-averaged currents in primary flow direction and floodgate discharges (a) respectively wind component in primary flow direction (b-d) and their dependency on shifts in time (a-c) and wind direction (d). The wind-current correlation figure (b) is for ADCP1 in channel F, figure (c) is for ADCP2 in channel D. The wind-current correlation has been investigated using wind averaged over the preceeding 10 min, 1 h, 3 h and 6 h.

References

Bowen, M.M., Geyer, W.R., 2003. Salt transport and the time-dependent salt balance of a partially stratified estuary. J. Geophys. Res. 108 (C5), 3158. https://doi.org/10.1029/2001JC001231.

Chen, S.-N., Sanford, L.P., 2009. Axial wind effects on stratification and longitudinal salt transport in an idealized, partially mixed estuary. J. Phys. Oceanogr. 39 (8), 1905–1920. https://doi.org/10.1175/2009JPO4016.1.

Chatwin, P.C., 1976. Some remarks on the maintenance of the salinity distribution in estuaries. Estuar. Coast Mar. Sci. 4, 555–566.

Csanady, G.T., 1975. Hydrodynamics of large lakes. Annu. Rev. Fluid Mech. 7, 357–386.

Deltacommissie, 2008. Working Together with Water: A Living Land Builds for its Future. Findings of the Delta Commissie 2008, Summary and Conclusions. http://deltacommissie.com/doc/deltareport_summary.pdf.

Ferguson, H.A. (Ed.), 1971. De afsluiting van het Haringvliet, documentatiereeks bouwen en baggeren, deel I (in Dutch). http://resolver.tudelft.nl/uuid:c496986c-efb3-4660-97f2-8fd76c6ac57b.

Figueroa, S.M., Lee, G., Chang, J., Lagamayo, K.D., Jung, N.W., 2021. Impact of estuarine dams on the estuarine parameter space and sediment flux decomposition: idealized numerical modeling study. Earth Space Sci. Open Arch. https://doi.org/10.1002/essoar.10507777.1.

Fischer, H.B., 1976. Mixing and dispersion in estuaries. Annu. Rev. Fluid Mech. 8, 107–133.

Fischer, H.B., 1972. Mass transport mechanisms in partially stratified estuaries. J. Fluid Mech. 53, 671–687. https://doi.org/10.1017/S0022112072000412.

Fischer, H.B., List, E.J., Koh, R.C.Y., Imberger, J., Brooks, N.H., 1979. Mixing in Inland and Coastal Waters. Academic Press, p. 483.

Fioole, A., 2020. Analyseren Meetgegevens Haringvliet – Nalevering. Memo 2020.07.

Geyer, W.R., Trowbridge, J.H., Bowen, M., 2000. The dynamics of a partially mixed estuary. J. Phys. Oceanogr. 30, 2035–2048.

Geyer, R., 1997. Influence of wind on dynamics and flushing of shallow estuaries. Estuarine Coastal Mar. Sci. 44, 713–722.

Geyer, W.R., MacCready, P., 2014. The estuarine circulation. Annu. Rev. Fluid Mech. 46, 175–197.

Hansen, D.V., Rattray, M., 1965. Gravitational circulation in straits and estuaries. J. Mar. Res. 23, 104–122.

Hearn, C.J., Hunter, J.R., Heron, M.L., 1987. The effects of a deep channel on the wind-induced flushing of a shallow bay or harbor. J. Geophys. Res. 92 (C4), 3913–3924. https://doi.org/10.1029/JC092iC04p03913.

Huismans, Y., 2016. Systeemanalyse Rijn-Maasmonding: analyse relaties noord- en zuidrand en gevoeligheid stuurknoppen. Deltares report 1230077-001, Delft, p. 73 (in Dutch).

Hunter, J.R., Hearn, C.J., 1987. Lateral and vertical variations in the wind-driven circulation in long, shallow lakes. J. Geophys. Res. 92 (C12), 13106–13114. https://doi.org/10.1029/JC092iC12p13106.

Imberger, J., Hamblin, P.F., 1982. Dynamics of lakes, reservoirs and cooling ponds. Annu. Rev. Fluid Mech. 14, 153–187.

Jun, K.S., Hwang, J.H., Kim, D.H., 2019. Numerical simulation of sea water intrusion due to partial gate opening of the Nakdong Estuary Dam. In: Sustainable and Safe Dams Around the World, ISBN 9780429319778. https://doi.org/10.1201/9780429319778-131.

Kang, X., Xia, M., Pitula, J.S., Chigbu, P., 2017. Dynamics of water and salt exchange at Maryland Coastal Bays. Estuar. Coast Shelf Sci. 189, 1–16. https://doi.org/10.1016/j.ecss.2017.03.002.

Kato, H., Phillips, O.M., 1969. On the penetration of a turbulent layer into a stratified fluid. J. Fluid Mech. 37, 643–655.

Kranenburg, W.M., 2020. Desalinisation Deep Pits: Relations Floodgate Discharge, Wind, Flow Velocities, Pycnocline Levels (In Dutch). Deltares report 11205272-021, Delft, p. 50.

Lange, X., Klingbeil, K., Burchard, H., 2020. Inversions of estuarine circulation are frequent in a weakly tidal estuary with variable wind forcing and seaward salinity fluctuations. J. Geophys. Res.: Oceans 125, e2019JC015789. https://doi.org/10.1029/2019JC015789.

Lee, K.H., Rho, B.H., Choi, H.J., Lee, C.H., 2011. Estuary classification based on the characteristics of geomorphological features, natural habitat distributions and land uses. Sea 16 (2), 53–69. https://doi.org/10.7850/jkso.2011.16.2.053.

Li, Y., Li, M., 2011. Effects of winds on stratification and circulation in a partially mixed estuary. J. Geophys. Res. 116, C12012 https://doi.org/10.1029/2010JC006893.

Morris, R.K.A., 2013. Geomorphological analogues for large estuarine engineering projects: a case study of barrages, causeways and tidal energy projects. Ocean Coast Manag. 79, 52–61.

Mortimer, C.H., 1953. The resonant response of stratified lakes to wind. Schweiz. Z. Hydrol. 15, 94–151. https://doi-org.tudelft.idm.oclc.org/10.1007/BF02486219.

National Research Council, 2014. Reducing Coastal Risks on the East and Gulf Coasts. The National Academies Press, Washington DC.

Officer, C.B., 1976. Physical Oceanography of Estuaries (And Associated Coastal Waters). John Wiley and Sons, Inc., New York xii + 465 pp.

Orton, P.M., Ralston, D.K., 2018. Preliminary Evaluation of the Physical Influences of Storm Surge Barriers on the Hudson River Estuary. Report to the Hudson River Foundation.

Price, J., 1979. On the scaling of stress-driven entrainment experiments. J. Fluid Mech. 90, 509–529.

Purkiani, K., Becherer, J., Klingbeil, K., Burchard, H., 2016. Wind-induced variability of estuarine circulation in a tidally energetic inlet with curvature. J. Geophys. Res. 121, 3261–3277. https://doi.org/10.1002/2015JC010945.

Ralston, D.K., 2022. Impacts of storm surge barriers on drag, mixing, and exchange flow in a partially mixed estuary. J. Geophys. Res. 127 https://doi.org/10.1029/2021JC018246.

Scully, M.E., 2010. Wind modulation of dissolved oxygen in Chesapeake Bay. Estuar. Coast 33 (5), 1164–1175. https://doi.org/10.1007/s12237-010-9319-9.

Scully, M.E., Friedrichs, C.T., Brubaker, J.M., 2005. Control of estuarine stratification and mixing by wind-induced straining of the estuarine density field. Estuaries 28, 321–326.

Signell, R.P., Beardsley, R.C., Graber, H.C., Capotondi, A., 1990. Effect of wave-current interaction on wind-driven circulation in narrow, shallow embayments. J. Geophys. Res. 95, 9671–9678. https://doi.org/10.1029/JC095iC06p09671.

Thompson, R.O.R.Y., Imberger, J., 1980. Response of a numerical model of a stratified lake to wind stress. Proc. 2nd Intl Symp. Stratified Flows, Trondheim, June 1980 1, 562–570.

Tönis, I.E., Stam, J.M.T., Van de Graaf, J., 2002. Morphological changes of the Haringvliet estuary after closure in 1970. Coast Eng. 44 (3), 191–203.

Valle-Levinson, A., 2010. Definition and classification of estuaries. In: Valle-Levinson, A. (Ed.), Contemporary Issues in Estuarine Physics. Cambridge Univ. Press, Cambridge, UK, pp. 1–11.

Watson, I., Finkl, C.W., 1990. State of the art in storm-surge protection: The Netherlands Delta Project. J. Coast Res. 6 (3), 739–764.

Weisberg, R.H., 1976. The nontidal flow in the Providence River of Narragansett Bay: a stochastic approach to estuarine circulation. J. Phys. Oceanogr. 6, 721–734.

Wong, K.C., 1994. On the nature of transverse variability in a coastal plain estuary. J. Geophys. Res. 99, 14, 209–14 222.

Wüest, A., Lorke, A., 2003. Small-scale hydrodynamics in lakes. Annu. Rev. Fluid Mech. 35, 373–412. https://doi.org/10.1146/annurev.fluid.35.101101.161220, 2003.

Xia, M., Xie, L., Pietrafesa, L.J., Whitney, M.M., 2011. The ideal response of a Gulf of Mexico estuary plume to wind forcing: its connection with salt flux and a Lagrangian view. J. Geophys. Res. 116, C08035 https://doi.org/10.1029/2010JC006689.

Zhu, Q., Wang, Y.P., Gao, S., Zhang, J., Li, M., Yang, Y., Gao, J., 2017. Modeling morphological change in anthropogenically controlled estuaries. Anthropocene 17, 70–83. https://doi.org/10.1016/j.ancene.2017.03.001.